ORIGINAL RESEARCH

Improving the Barrier Properties of Food Packaging by $Al_2O_3@TiO_2$ & $Al_2O_3@SiO_2$ Nanoparticles

Samaneh Tavakolian[1] · Hamed Ahari[2] · Mohammad Hadi Givianrad[3] · Hedayat Hosseini[4]

Abstract

The film or coating is one of the vital components in food packaging systems; thereby, it is necessary to promote them with potent functions. Nanocomposite films based on carboxymethyl cellulose (CMC) containing $Al_2O_3@SiO_2$ and $Al_2O_3@TiO_2$ nanoparticles were obtained by casting techniques. The synthesized materials were characterized by their morphology, size, and structure. Moisture absorption (MA), water vapor permeability (WVP), and gas transmission rate (GTR) were also measured to study the barrier properties of films. According to the results, the core-shell nanoparticles showed a smaller diameter, uniform dispersion, and no accumulation in the film matrix compared to the alumina allotropes (γ-,η-,α-Al_2O_3). The presence of $Al_2O_3@SiO_2$ and $Al_2O_3@TiO_2$ nanoparticles significantly regulated MA, WVP, and GTR compared to the allotropes. The most significant reduction in MA, WVP, and GTR belonged to the γ-$Al_2O_3@SiO_2$ (2.11%), η-$Al_2O_3@TiO_2$ (6.09×10^{-10} g/m s pa), and η-$Al_2O_3@TiO_2$ (0.21 cm^3/m^2d bar) respectively. To sum up, embedding core-shell nanoparticles within the matrix of polymeric films (CMC) can be a good idea to increase the efficacy of food packaging systems.

Keywords Food packaging · Core-shell nanoparticle · Alumina · Carboxymethyl cellulose · Nanocomposite

Introduction

Food packaging (FP) is one of the most important aspects of the modern food industry, and just a few food products are sold without packaging. Among the positive effects of a good package is prevention of wastage (Moeller and Matyjaszewski 2012), long shelf-life (Blanco 2016), and easy transportation (Robertson 2014; Lipińska et al. 2019). Shelf-life is known as the most important item in novel FP systems (García-García et al. 2013).

Food shelf life is affected by several factors such as chemical, physical, and microbial processes, which leads to a significant reduction in consumer acceptance (Hosseini and Jafari 2020). Barrier properties as one of the main properties in FP have been also considered to approve a new FP system. Development of FP with improved barrier properties (liquid and gas) in FP by modifying their microstructure can be one of the most significant achievements in food shelf life enhancement (Sanchez-García 2011). It is possible to control the barrier properties by embedding nanomaterials within the film structure (Sangroniz et al. 2019).

Nanomaterials, due to their small particle size and high surface area in relation to volume and specific properties in comparison with bulk materials, have been identified as potent candidates for various applications such as microelectronics, medicine, agriculture, foods, energy harvesting, and environmental applications (Challagulla et al. 2020; Chen et al. 2020; Rawtani et al. 2020). Nanoscience and nanotechnology have become exciting fields of research and development in different fields of food microbiology and food science, such as FP, food processing, food-borne pathogens detection, development of functional food, food safety, and shelf-life extension of food (Neethirajan and Jayas 2011; Singh et al. 2017)

✉ Hamed Ahari
dr.h.ahari@gmail.com

[1] Department of Food Science, Science and Research Branch, Islamic Azad University, Tehran, Iran

[2] Department of Food Science and Technology, Science and Research Branch, Islamic Azad University, Tehran, Iran

[3] Department of Chemistry, Science and Research Branch, Islamic Azad University, Tehran, Iran

[4] Department of Food Science and Technology, National Nutrition and Food Technology Research Institute, Faculty of Nutrition Sciences and Food Technology, Shahid Beheshti University of Medical Sciences, Tehran, Iran

considering their impact on the film barrier properties and microorganism growth.

Integration of nanomaterial with biomaterials revealed noticeable progress in improving the barrier properties in FP (Siracusa et al. 2012; Nakajima et al. 2017). The bio-nanocomposites are made of bio-polymers comprising two vital components: (a) biopolymer which acts as a matrix and the continuous phase and (b) reinforcement agent which is known as the dispersed phase with the size of 1–100 nm (Kumar et al. 2020; Sharma et al. 2020). The dispersed phase includes different kinds of nanoparticles (Souza and Fernando 2016) and nanoemulsion (Aswathanarayan and Vittal 2019) which not only promote the barrier properties but also prevent spoilage by controlling bacteria growth, improving mechanical and physico-chemical properties of the packaging (Das et al. 2020). Numerous nanoparticles are employed in novel FP systems as dispersed phase which showed high impact on barrier properties improvement (Zhong et al. 2017; Amjadi et al. 2019; Biswal and Misra 2020; Ernest Ravindran et al. 2020; Saravanakumar et al. 2020). For instance, Polyhedral oligomeric silsesquioxane (POSS) integrated with the low density polyethylene (LDPE)-based nanocomposite films showed noticeable potential in the shelf life extension of minced beef (Kavuncuoglu et al. 2019).

Increasing the surface area of the nanoparticles showed a significant impact on their efficacy specifically boosting the barrier properties (Ahangaran and Navarchian 2020). Core-shell nanoparticles (CSNs) are known as diverse and unique means of transport for bioactive compounds while increasing the surface area (Blanco-Pascual et al. 2014; Ahangaran and Navarchian 2020). In the most of studies, nanoparticles have been employed in FP in their common and simple form. As another but rare distinct form of metals in FP is bimetallic and trimetallic nanoparticles which are in the form of core-shell nanoparticles or alloy nanoparticles (Basavegowda et al. 2020) (Mohsin et al. 2020). These forms of nanoparticles are well-known in other industries including catalyst production water purification (Ghosh et al. 2020; Zhao et al. 2020).

Based on our literature review, it can be hypothesized that the integration of CSNs with biomaterials for food packaging purposes may increase food shelf-life by improving physico-chemical properties of films including the barrier properties. Hence, this study aims to synthesize different allotropes of alumina coated with SiO_2 and TiO_2 as CSN nanoparticles separately to enhance the efficiency of Food Packaging films. SiO_2 and TiO_2 were employed in FP extensively but in their free form as single nanoparticles (Zhu et al. 2018; Zhu et al. 2019; Wang et al. 2020). These nanoparticles are neutral, non-toxic, environmentally friendly, and inexpensive, and have antimicrobial properties against a large number of microorganisms. This study has been carried out to increase their potent in FP by producing their CSN form.

Material and Methods

Materials

The chemicals such as $Al(NO_3)_3.6H_2O$ (99% w/w), ethanol, ammonia, Carboxymethyl cellulose (CMC), and glycerol were all products of Merck and in analytical grade and purchased from the local supplier (Temadkala). The SiO_2 and TiO_2 nanoparticles were provided by Aimina Co. (Tehran, Iran). All the chemicals were analytical grade and used without any further purification.

### Synthesis of Nanomaterials

Al_2O_3

First of all, 6.07 g of $Al(NO_3)_3.6H_2O$ was dissolved in a mixture of 24 mL of water and 8 mL of ethanol. Then, 12.29 mL of ammonia (15 M) was slowly added dropwise. During the addition of ammonia, the color of the solution became cloudy, indicating the formation of aluminum hydroxide. Then, the resulting mixture was placed in a container and was placed in an oil bath at 85 °C for 24 h. In following, to remove the remained aluminum nitrate, the obtained gel was rinsed with distilled water and centrifuged (10000 rpm: 15 min). This step was repeated two times. The resulted gel was rinsed with ethanol to remove the residual water. Finally, the gel was dried in furnace (SHIMAZ Co., Tehran, Iran) at 100 °C for 24 h.

α-, η-, γ-Al_2O_3

To synthesize α-Al_2O_3, η-Al_2O_3, and γ-Al_2O_3, the synthesized powder was placed in a furnace at 1200, 750, and 500 °C respectively with a heating rate of 2 °C/min for 4 h. The heating rate must be low to prevent the solvent from escaping rapidly and destroying the cavities.

$Al_2O_3@TiO_2$ and $Al_2O_3@SiO_2$

$Al_2O_3@SiO_2$ was synthesized according to the "Al2O3" section with a little modification. 6.07 g of $Al(NO_3)_3.6H_2O$ was dissolved in water/ethanol solution (3:1% v/v), which was mentioned previously. Then, 0.25 g of SiO_2 nanoparticles was added and stirred for 30 min at room temperature. Subsequently, 12.29 mL of 15 M ammonia was added dropwise. The color of the solution became milky due to the aluminum hydroxide formation. Then, the resulting mixture was transferred to a container and placed in an oil bath at 85 °C for 24 h. Following the steps in "Al_2O_3" section, finally, the gel was dried in furnace at 100 °C for 24 h. The synthesis steps are shown schematically in Fig. 1. The same procedure was followed to synthesize $Al_2O_3@TiO_2$ by adding 0.25 g TiO_2 instead of SiO_2.
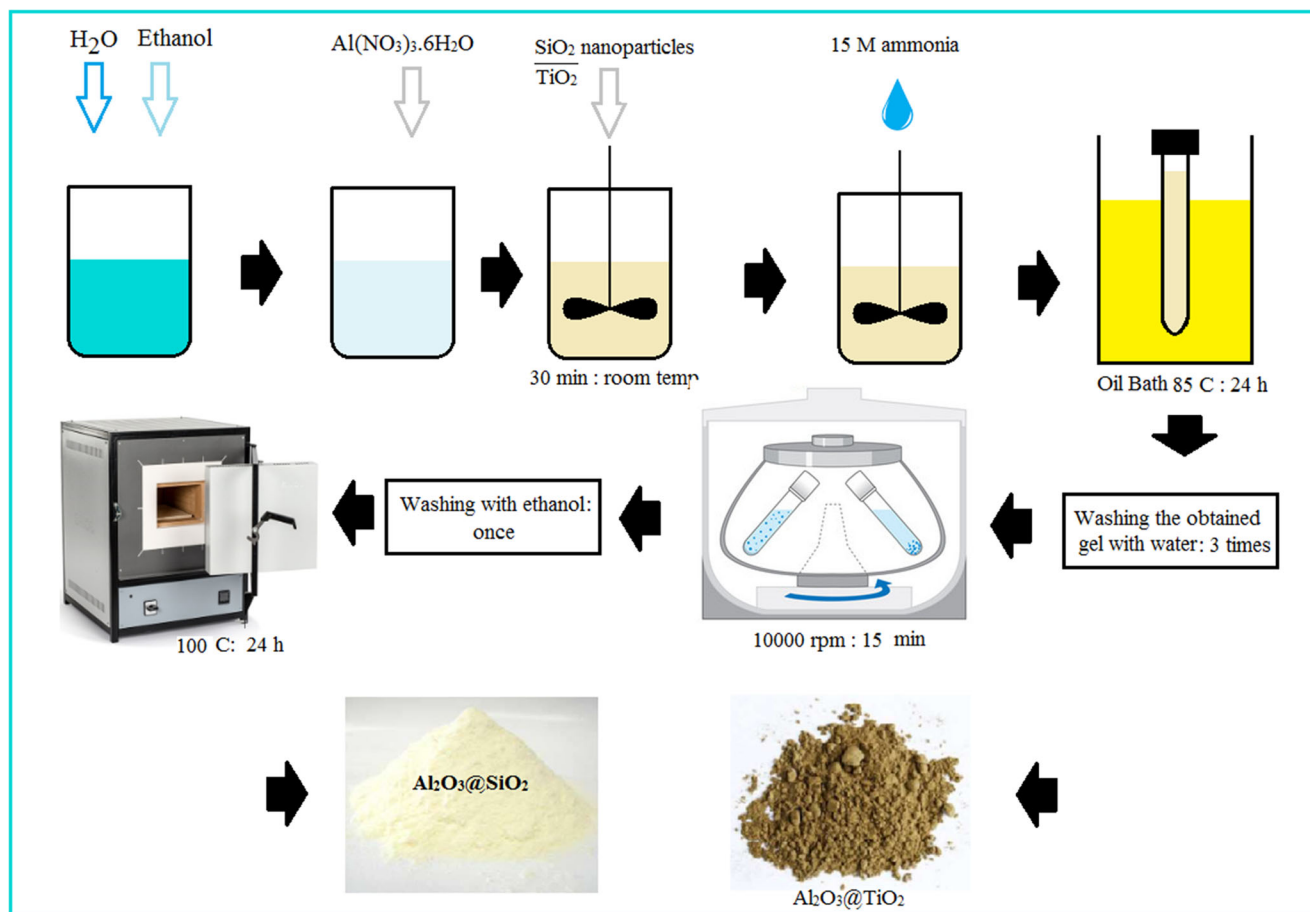
Fig. 1 Flow diagram of $Al_2O_3@SiO_2/Al_2O_3@TiO_2$ synthesis

α-,γ-,η-Al$_2$O$_3$@SiO$_2$ and α-,γ-,η-Al$_2$O$_3$@TiO$_2$

According to the "α-, η-, γ-Al2O3" section, to synthesize α-$Al_2O_3@SiO_2$, η-$Al_2O_3@SiO_2$, and γ-$Al_2O_3@SiO_2$, an appropriate amount of $Al_2O_3@SiO_2$ was calcined at 1200, 750, and 500 °C for 4 h respectively. The heating rate was adjusted as 2 °C/min.

Preparation of Films Containing Nanoparticles

Twenty milligrams of the prepared nanoparticle was dispersed in 100 mL distilled water using ultrasonicator (TOPSONIC, Tehran, Iran). Then, 1 g of CMC was added and dissolved at 80 °C and using magnetic stirrer (1200 rpm). Then, 0.5 g of glycerol was added to the solution as a lubricant and stirred for 30 min. In order to cool and completely remove the air bubbles, the solution was degassed for 5 min in an ultrasonic bath with a power of 60 MHz and then left at room temperature. Next, the polymeric solution was casted in a petri dish (d: 15 cm) to remove the water content. The plates were placed in oven at 40 °C. After 24 h, the films were removed from the plate and kept in a refrigerator. The thickness of the prepared films was 0.5 millimeter.

Instrumental Characterization

Fourier-Transform Infrared Spectroscopy Analysis

The chemical bonds and molecular structure of the nano-sized samples were evaluated by Fourier transform infrared spectroscopy (FTIR, BRUKER TENSOR II, Germany). The IR spectrum appeared in the wavelength range 500 to 4000 cm^{-1}.

X-Ray Diffraction Analysis

To detect the phase compositions of the prepared samples, X-ray diffraction (Bruker D8

Advanced XRD, Bruker AXS Inc., Madison, WI) analyses were carried out using Bruker D8 Advance X-ray diffractometer equipped with LYNXEYEXE-T detector. The diffractograms were collected in the 2θ range from 10 to 80° with a scanning rate of 2°/min. The results of X-ray diffraction spectrometer were analyzed using X'Pert High Score Ver.2.2 software. Finally, by comparing the information about nanoparticles with the standard data in the ICCD-PDF2/PDF4 software library, which belongs to the year 2004, their phase was identified and determined.

Field Emission Scanning Electron Microscopy Analysis

The morphology and size of the synthesized nanoparticles were investigated using field emission scanning electron microscopy at accelerating voltages of 15 kV and working distance of 5 mm with different magnification (FE-SEM, MIRA III, TESCAN Co., the Czech Republic). The synthesized nanoparticles were coated directly with gold.

Moisture Absorption

To measure moisture absorption (MA), the prepared films were dried in an oven (40 °C) for 24 h and then cooled down in a desiccator. Immediately they were weighed. Next, the dried films were emerged in the water at room temperature for 24 h. Finally, films were taken from the water, removed the residual water, and weighed (Shen and Springer 1976).

Water Vapor Permeability

Gravimetric techniques are usually employed to measure water vapor permeability (WVP). The WVP test was performed according to the ASTM E96-95 standard. In this method, glass vials with a specific diameter and the same apparent dimensions were employed. Ten milliliters of distilled water was poured into the vials to create 100% humidity, and the film samples were placed on the lid of the vials and secured with glue and plastic washers. These vials were then weighed and then transferred into a desiccator and their weight loss was determined by weighing them at different intervals. The WVP was calculated by the following Eqs. (1) and (2):

$$WVPR = \frac{\Delta m}{\Delta t}/A \tag{1}$$

in which:

WVPR	water vapor permeability rate (g/m^2.s)
Δt	time interval (t)
Δm	weight difference in Δt (g)
A	area of the film (m^2)

$$WVP = \frac{WVPR}{P} \times X \tag{2}$$

in which:

WVP	water vapor permeability (g/m s Pa)
P	pure water vapor pressure at 25 °C (Pa)
X	thickness of the films (m)

Gas Transmission Rate (GTR)

Gas transmission rate (GTR) is calculated by measuring the volume of gas (oxygen) passing through the film (coating) per unit time and area (Mrkić et al. 2006). GTR of films measured according to ASTM D1434 standard, using GDP-C gas permeability tester (Coesfeld Meteriatest, Germany).
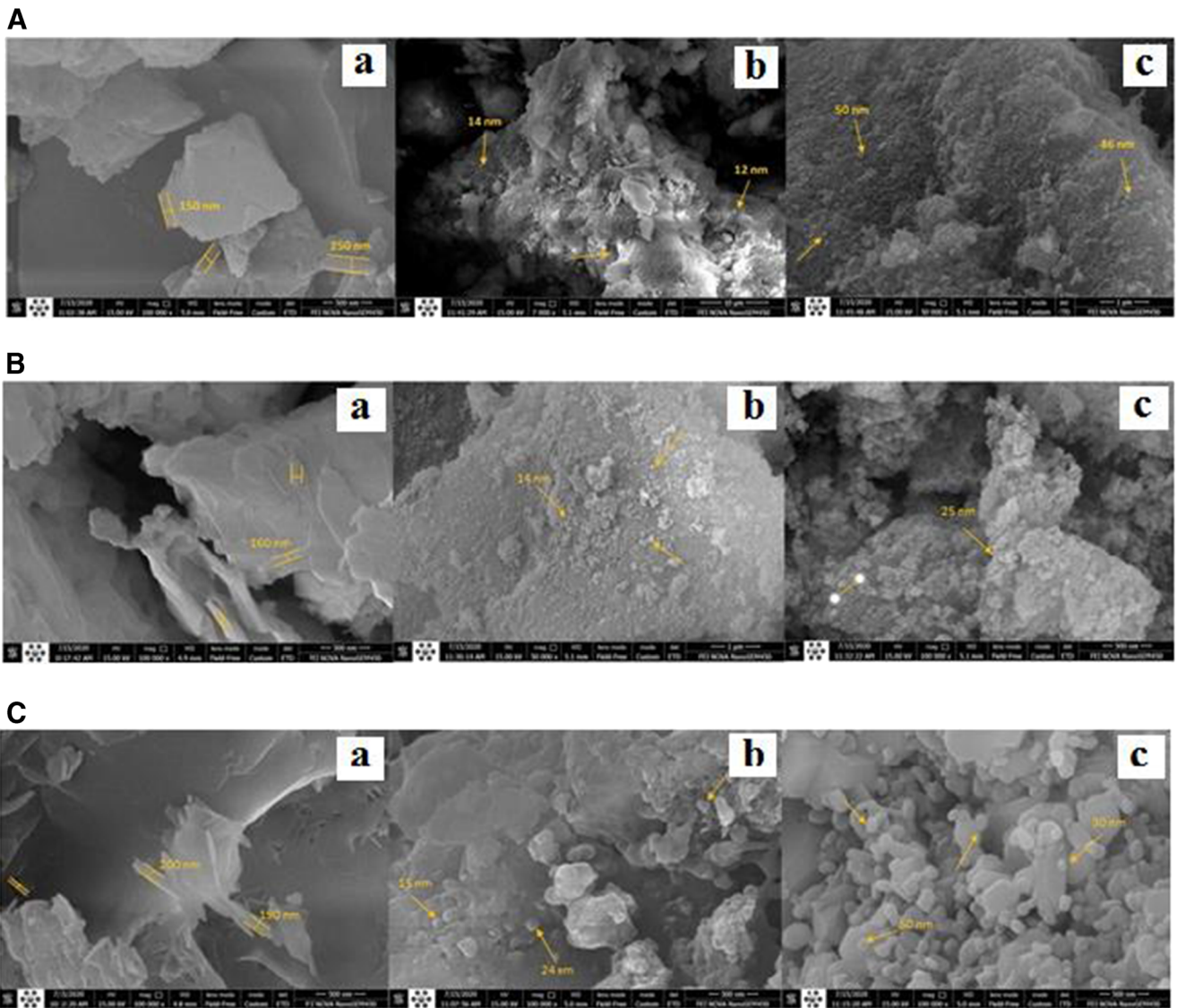
Results and Discussion

To promote the quality of food packaging films, CSN Al_2O_3 nanoparticles were embedded in CMC film. SiO_2 and TiO_2, like shell, were deposited on the surface of the various allotropes of Alumina including α, η, γ type, and then mixed in CMC before film preparation. The production of nanoparticles, their morphology, and their effect on food packaging film improvement were evaluated by analytical and experimental studies.
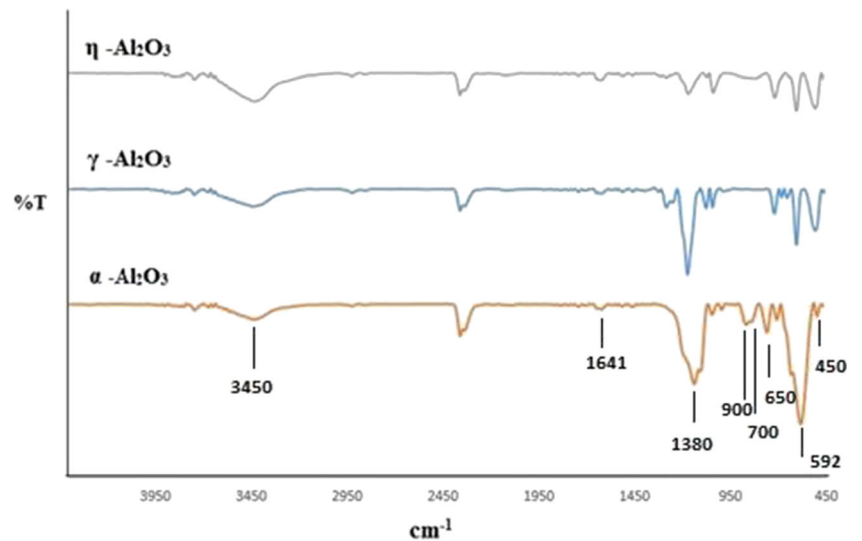
Synthesis of Nanoparticles

The shape and size distribution of the synthesized nanoparticles were characterized using scanning electroscope microscope (SEM). According to the obtained FE-SEM images of the nanoparticles (Fig. 2), the average particle size is in the range of 15–250 nm and no large particles were formed (López-Juárez et al. 2018). Therefore, with increasing surface area, intermolecular collisions, and finally the reaction speed increases (Jafari et al. 2017). With the formation of γ-Al_2O_3 (Fig. 2A (a)), η-Al_2O_3 (Fig. 2B (a)), and α-Al_2O_3 (Fig. 2C (a)), the particle size increased slightly, respectively, and the morphology turns into accumulation. According to Fig. 2, the crystal particle sizes of different allotropes of alumina nanoparticles without coating are in the range of 250–150 nm (Fig. 2ABC (a)), Al_2O_3-SiO_2 nanoparticles are in the range of 14–25 nm (Fig. 2ABC (b)), and Al_2O_3-TiO_2 nanoparticles are in the range of 25–50 nm (Fig. 2ABC (c)). It shows that using SiO_2 as a shell (core@SiO_2) leads to smaller and uniform nanoparticles with the same morphology in all kinds of allotropes compared with TiO_2 (core@TiO_2). Generally, as the particle size decreases, the surface area increases. Therefore, it was hypothesized that intermolecular collisions and finally the reaction speed increase. Nanoparticles of core@SiO_2 showed more agglomeration in contrast with core@TiO_2.

Figure 3 depicts the FTIR spectra for α-Al_2O_3, η-Al_2O_3, and γ-Al_2O_3 nanoparticles in the range of 400–4000 cm^{-1}. Following the same trend, similar peaks appeared at 450, 592, 650, 700, 900, 1380, 1641, and 3450 cm^{-1}. The peaks that appeared in the wavelength range of 650–450 cm^{-1} related to the strength vibrations of the octahedral of the site. Thereby, the wide peak that appeared at 592 cm^{-1} could be attributed to Al-O stretching modes in the octahedral structure

Fig. 2 FE-SEM images for **A** (a) γ-Al$_2$O$_3$; (b) γ-Al$_2$O$_3$@SiO$_2$; (c) γ-Al$_2$O$_3$@TiO$_2$, **B** (a) η-Al$_2$O$_3$; (b) η-Al$_2$O$_3$@SiO$_2$; (c) η-Al$_2$O$_3$@TiO$_2$, **C** (a) α-Al$_2$O$_3$; (b) α-Al$_2$O$_3$@SiO$_2$; (c) α-Al$_2$O$_3$@TiO$_2$

Fig. 3 FTIR spectra of α, η, and γ-Al$_2$O$_3$

(Prashanth et al. 2015). On the other hand, the peaks that appeared in the range of 700–900 cm^{-1} are related to the strength vibrations of tetrahedral AlO_4 species. The peak in the 1380 cm^{-1} was related to the adsorption of the OH group (caused by the adsorbed water molecules by the nanoparticles from moisture). The appeared weak band at 2350 cm^{-1} was attributed to the C–H bond stretching vibration of the methyl group in urea (Baghani et al. 2015; Farahmandjou and Golabiyan 2015; Prashanth et al. 2015).

Figure 4 a and b show the FTIR spectra for core@SiO_2 and SiO_2 nanoparticles respectively in the range of 400–4000 cm^{-1}. As it can be seen in Fig. 4a, γ-Al_2O_3@SiO_2, α-Al_2O_3@SiO_2, η- Al_2O_3@SiO_2 showed similar trends in the same wavelength. The band appeared at 459 cm^{-1} (Fig. 4a) and at 466 cm^{-1} (Fig. 4b) attributed to Si-O-Si bending modes. As it can be seen, after core@ SiO_2 production, the peak shifted from 455 to 466 and decreased in the area, which shows its attachment to the core. Also, the spectrum related to the wavenumber 807 cm^{-1} shows the stretching vibration modes of the Si-O-Si bond (Nithiyanantham et al. 2019), and the spectra related to the 1074 and 1220 cm^{-1} are related

to the asymmetric stretching modes of Si-O-Si (Ewing et al. 2014). The presence of the SiO_2 characteristic bands is clearly observed in the region of 1220–950 cm^{-1} which approve the formation of the γ-Al_2O_3@SiO_2, α-Al_2O_3@SiO_2, η-Al_2O_3@SiO_2 CSNs (Ding et al. 2012).

Similarly, considering core@TiO_2, the appeared spectrum about 483 cm^{-1} is related to the vibrations of the Ti-O bond (Fig. 4c, d) (Mugundan et al. 2015). Ti-O flexural vibrations are also observed in the 1630 cm^{-1} region (Choudhury and Choudhury 2012). Comparing Fig. 4c and Fig.4d, reduction in the area under the corresponding peak at 483 cm^{-1} and appearing a wide band around 1200 cm^{-1} reveals the interaction between core and shell (TiO_2). This interaction happened extensively about η-Al_2O_3 compared to other allotropes.

Figure 5 shows the X-ray diffraction pattern of the synthesized alumina at 550, 750, and 1200 °C. According to Fig. 5a, the appeared peaks at X and Y confirmed the existence of the Al_2O_3 phase and conformity of the obtained pattern with the standard gamma-alumina card pattern available in the X'Pert High Score Plus software library number (No. ICDD-01-075-0921) (Thümmler et al. 2019). The peaks observed at angles
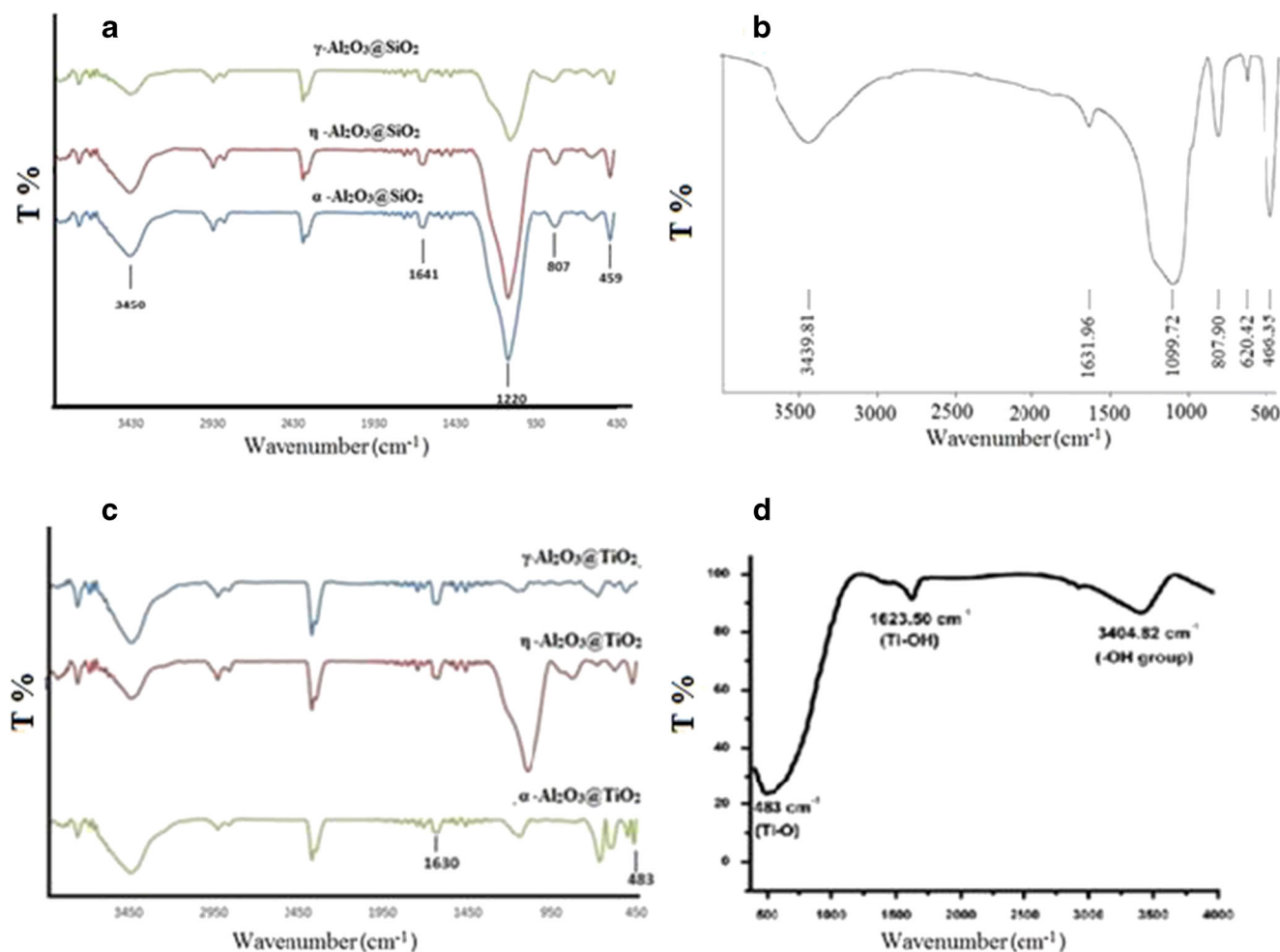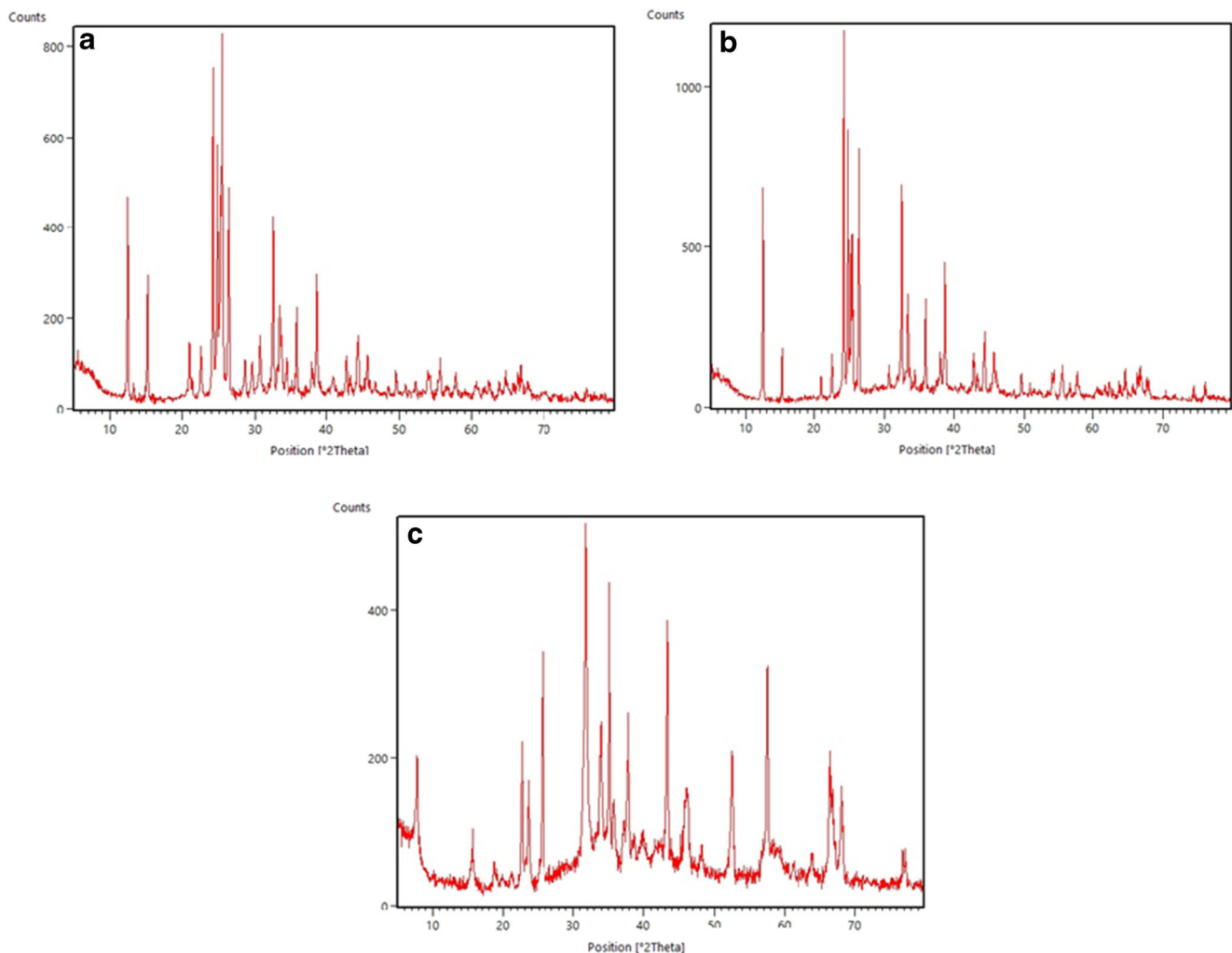

Fig. 4 FTIR spectra for **a** Core@SiO_2, **b** SiO_2, **c** Core@TiO_2, and **d** TiO_2 (Chougala et al. 2017)

Fig. 5 XRD patterns of **a** γ-Al$_2$O$_3$, **b** η-Al$_2$O$_3$, and **c** α-Al$_2$O$_3$

45.6° and 67.1° confirm the η-phase (Fig. 5b). The same results were addressed by others (Wynnyckyj and Morris 1985; Habibi and Dufresne 2008; Szkodo et al. 2016). The result is in agreement with the standard η-Al$_2$O$_3$ card template available in the software library (No. JCPDS 04-0875). The result corresponds to the standard α-Al$_2$O$_3$ card pattern in the software library (No. ICDD-01-075-0783). The prepared phase has a rhombohedral structure. The oxygen anions form a compact hexagonal lattice (hcp) and the aluminum cations are in octahedral positions. The peaks in this structure are very sharp, which indicates the high crystallinity of the alpha structure compared to the gamma phase (Fig. 5c) (Sun et al. 2003).

The prepared phase has a cubic structure in which the oxygen anions of the cubic lattice form the center of charge, and the aluminum cations occupy the octahedral and tetrahedral positions. Gamma alumina is a two-phase system consisting of cubic gamma-alumina and tetragonal gamma-alumina. The tetragonal phase is predominant at low temperatures and the cubic phase is predominant at higher temperatures, so the rate of tetragonal deviation decreases with increasing calcification temperature.

As it can be seen in Fig. 6a, two phases of Al$_2$O$_3$ (2 38°, 45°, 67°) and SiO$_2$ (2 22°) were detected (Okuno et al. 2005). Considering all allotropes, wide peaks corresponding to SiO$_2$ nanoparticles were observed around 22°, and the SiO$_2$ diffraction pattern showed an amorphous phase and the appeared peaks of Al$_2$O$_3$ revealed crystal structures (Kusumawati et al. 2018). The obtained results were in agreement with the standard SiO$_2$ card pattern available in the software library (No. PDF 01-086-1628) (Nallathambi et al. 2011). Shifting peaks and the various diffraction trends between core@SiO$_2$ and the basic data (standard allotropes of Al$_2$O$_3$) are hypothesized to be affected by the process and the core material of the γ-, η-, α-Al$_2$O$_3$ phase formation (Wu et al. 2016).

Based on Fig. 6b, Al$_2$O$_3$ and TiO$_2$ were the two detected phases around the angels of (26°, 36°, 57°, 68° at angles of 28°, 38°, 48°, 54.2°, 55.3°, and 63.8°, peaks related to TiO$_2$ nanoparticles detected, which indicates the presence of TiO$_2$ nanoparticles (Ali et al. 2018). The results were in agreement with the standard TiO$_2$ card pattern available in the software library (No. PDF 04-006-9240). Other peaks appearing at

Fig. 6 XRD patterns of (**a**) α-, η-, γ-Al$_2$O$_3$@SiO$_2$ and (**b**) α-, η-, γ-Al$_2$O$_3$@TiO$_2$
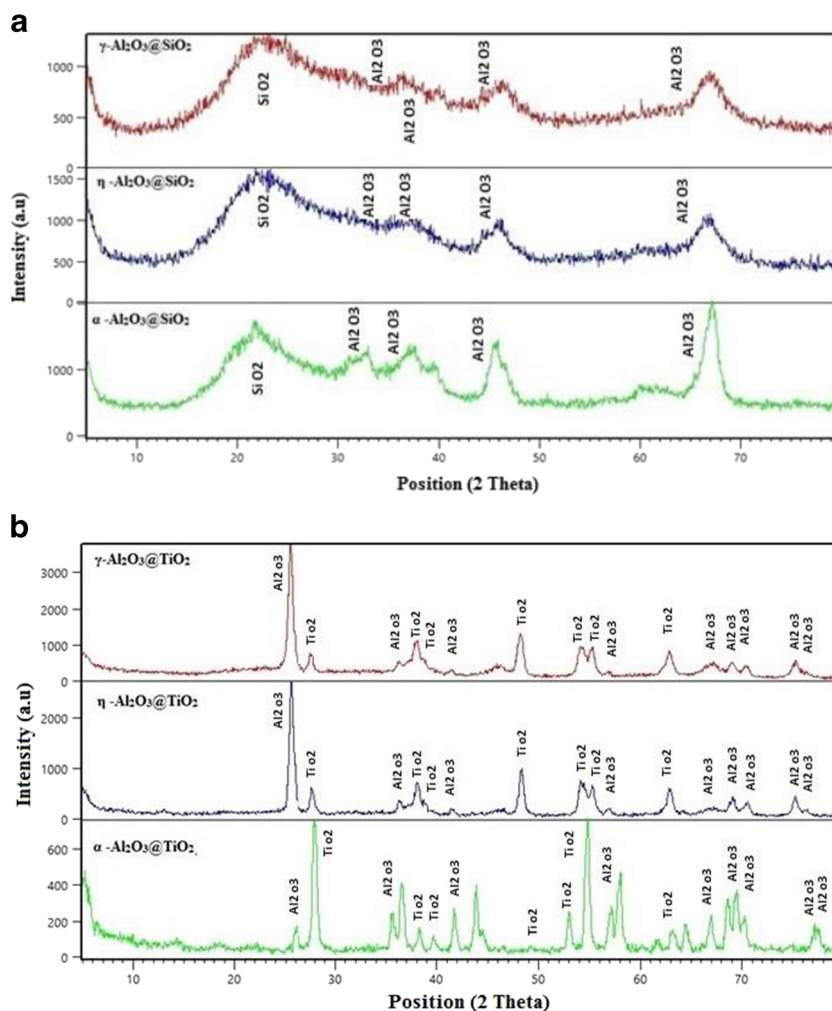
other angles proved the existence of gamma, beta, and alpha phases.

The temperature of aluminum hydroxide decomposition has been known, as a vital factor in the preparation technique. The different intensities can be attributed the process temperature.

MA determines the amount of water absorbed by the films (Gaikwad et al. 2018). Several factors including temperature, additives used, type of plastic, and length of exposure affect the level of MA (Wong and Rajoo 2003). On the other hand, one of the important parameters in choosing the materials for food packaging purposes is the relative humidity of the storage place. When the packaging film is highly sensitive to moisture, the humidity of the environment may negatively change the efficiency of the film due to moisture absorption, which results in qualitative and quantitative changes in foods (Khalilullah et al. 2018; Mishra et al. 2020) Based on Table 1, embedding nanoparticles of allotropes of alumina showed a significant difference compared with the control group (no nanoparticle) ($P <$ 0.05). Addition of core@shell nanoparticles revealed a significant reduction in MA in comparison with the control group ($P <$

0.01). Comparing each allotrope with TiO$_2$ and SiO$_2$ as shell, no significant difference was observed between them ($P > 0.05$) but γ-Al2O$_3$@SiO$_2$ ($P < 0.05$). Comparing the allotropes of each kind of shells (TiO$_2$ and SiO$_2$), in the case of SiO$_2$, no significant difference was observed. Between α and γ type ($P > 0.05$) while they showed a positive significant different with the η type ($P < 0.05$). Considering TiO$_2$, no significant difference observed ($P > 0.05$).

By embedding nanoparticles (α-,η-,γ-Al$_2$O$_3$; α-,η-,γ-Al$_2$O$_3$@SiO$_2$; α-,η-,γ-Al$_2$O$_3$@TiO$_2$) into the films, MA reduced from 30.84% (film without nanoparticles) to (α: 23.72%, 2.38%, and 3.51%), (η: 22.14%, 6.83%, 4.95%), and (γ: 15.96%, 2.11%, and 4.92) respectively. The addition of nanoparticles to the films significantly reduced the MA level ($P < 0.05$). The highest MA belonged to the pure or non-nanocomposite films (30.84%) and the lowest MA was attributed to the film containing α-Al$_2$O$_3$@SiO$_2$ and γ-Al$_2$O$_3$@SiO$_2$ core-shell nanoparticle. In the case of embedding allotropes, γ-Al$_2$O$_3$ showed a significant reduction in MA level. Considering embedding CSN, γ-Al$_2$O$_3$@SiO$_2$ and α-Al$_2$O$_3$@SiO$_2$ revealed a lower reduction in MA level.

Table 1 MA measurement for films incorporated with different types of Al_2O_3-based nanoparticles

Allotropes	MA % of films			
	Without nanoparticle	-Al_2O_3	-Al_2O_3@SiO_2	-Al_2O_3@TiO_2
α	30.84 ± 0.3 [aA]	23.73 ± 0.15 [bA]	2.38 ± 0.18 [cA]	3.51 ± 0.14 [cA]
η	30.48 ± 0.3 [aA]	22.14 ± 0.18 [bA]	6.83 ± 0.12 [cB]	4.95 ± 0.21 [cA]
γ	30.48 ± 0.3 [aA]	15.96 ± 0.21 [bB]	2.11 ± 0.16 [cA]	4.92 ± 0.20 [dA]

Same letters means no significant difference (P value > 0.05); different letters means significant difference (P value < 0.05). Compare the small letter in each row and the capital letters in each column

Comparing core@SiO_2 and core@TiO_2, γ-Al_2O_3@SiO_2 showed the most significant reduction in MA level.

The prepared alumina nanocomposites were able to increase the resistance of CMC-based film to moisture. Primarily, the moisture absorption of the film depends on the hydrophilic properties of the polymer and the presence of cavities and voids between the chains. For instance, the presence of hydroxyl groups in the chemical structure of CMC and glycerol affects the moisture absorption in the film by binding with water (Ergun et al. 2016). The presence of nanoparticles in films reduced the accessibility of hydroxyl groups to water molecules. The bonding and interaction between alumina nanocomposites reduce the free groups of CMC film and reduces the surface hydrophilicity, and in this regard can help to reduce MA. It is hypothesized that an increase in the concentration of nanoparticles may result in lower MA. On the other hand, silicon oxide and titanium oxide nanoparticles bond with their hydroxyl and carboxyl groups of CMC through their hydroxyl groups (Almasi et al. 2009), and creating a strong and cohesive structure by reducing the free space for moisture penetration can reduce the rate of moisture penetration into the film. The smaller the particle size, the better the effect (Cyras et al. 2008; Almasi et al. 2010). These results were in agreement with the previous studies (Dittanet et al. 2017), although it may alter the mechanical properties of the films (Khalilullah et al. 2018). By comparing the results in Table 1, it can be concluded that the addition of nanoparticles improved MA level. Besides, embedding CSNs within the film showed better improvement in comparison with simple allotropes. Comparing core@TiO_2 and core@SiO_2, employing TiO_2 showed better efficacy in MA adjustment. The reason might be attributed to the ability of TiO_2 in oxidizing molecules of H_2O into the hydroxyl group, which lowers the content of water (Lee et al. 2017). On the other hand, as previously mentioned about the role of nanoparticle size in MA level, because of the smaller diameter of TiO_2 and based on the SEM results (Fig. 2), smaller CSNs were produced by TiO_2 in contrast with SiO_2.

The formation of lattice structure due to strong hydrogen bonds of the polymer chain as well as strong hydrogen bonds between the particles of these nanoparticles and the polymer chain creates a cohesive, integrated, and potent structure with low porosity that decreases the penetration of moisture into the film. Scientists have also reported such networks of polysaccharide rod fillers. They reported that as the nanoparticle concentration increased, compact and crystalline structure developed, the pores between the chains were reduced, and as a result, the possibility of water molecules penetrating reduced, and the MA of the films decreased (Habibi and Dufresne 2008; Lin et al. 2011). Similar results were reported by Liu et al. (Liu et al. 1999) on reducing the MA of starch films by adding polyvinyl alcohol polymer to starch films. The scientists stated that with increasing polyvinyl alcohol at concentrations of 13, 18, 26, and 39%, the percentage of MA shows a decreasing trend. In another study, a reduction in MA of film due to an increase in the amount of nanoparticles from 25 to 75% was reported (Goetz et al. 2009).

One of the parameters of the film that has a great effect on the shelf life of fruits and foods is the rate of WVP. This factor determines the moisture transfer in different materials and is a very important parameter that affects the quality of the product (Choudhury and Choudhury 2012). If the purpose of the film is to package the food ingredients, the passage of water vapor through the film between the environment and the food texture must be minimized. This property is related to the properties of the film materials such as hydrophilicity or hydrophobicity of the constituent compounds, the amount and type of additive to the film, the presence of cracks and pores, and also the type of polymer structure (Turan 2019). Hence, it was hypothesized that the embedding of CSNs into the food packaging film will decrease its WVP. In Table 2, the WVP data for all composites with different nanoparticles were tabulated. As it can be seen, films with nanoparticles resulted in lower WVP than that of the control group. In the case of α type nanoparticles, α-Al_2O_3@SiO_2 showed a significant difference compared with the others ($P < 0.05$). However, no significant difference observed between films with α-Al_2O_3 and α-Al_2O_3@TiO_2 ($P > 0.05$). Regarding η type nanoparticles, η-Al_2O_3@TiO_2 depicted significant difference in comparison with the other groups ($p < 0.05$). η-Al_2O_3@SiO_2 showed no significant difference compared with η-Al_2O_3 ($P > 0.05$). Considering γ types films, no significant difference observed ($P > 0.05$). Comparing the allotropes (in column), no significant difference observed among α-Al_2O_3, γ-Al_2O_3, and η-

Table 2 WVP measurement for films incorporated with different types of Al$_2$O$_3$-based nanoparticles

Allotropes	WVP of Films (WVP × 1^{1-} [g/m s pa])			
	Without nanoparticle	-Al$_2$O$_3$	-Al$_2$O$_3$@SiO$_2$	-Al$_2$O$_3$@TiO$_2$
α	7.3 ± 0.15 [aA]	6.8 ± 0.22 [aA]	6.2 ± 0.15 [bB]	7.2 ± 0.20 [aA]
η	7.3 ± 0.15 [aA]	±0.22 [aA]6.94	±0.15 [aA]6.79	±0.18 [bB]6.09
γ	7.3 ± 0.15 [aA]	±0.24 [aA]6.68	±0.19 [aA]6.56	±0.25 [aA]6.44

Same letters means no significant difference (*P* value > 0.05); different letters means significant difference (*P* value < 0.05). Compare the small letter in each row and the capital letters in each column

Al$_2$O$_3$ (*P* > 0.05). α-Al$_2$O$_3$@SiO$_2$ revealed significant difference in comparison with η and γ-Al$_2$O$_3$@SiO$_2$ (*P* < 0.05). No significant difference was reported between γ-Al$_2$O$_3$@SiO$_2$ and η-Al$_2$O$_3$@SiO$_2$ (*P* > 0.05). Finally, η-Al$_2$O$_3$@TiO$_2$ showed significant difference in contrast with other allotropes including α and γ with TiO$_2$ as shell (*P* < 0.05).

The addition of nanoparticles improved WVP compared with the NP-free film (7.3 × 10^{-10} g/m s pa). Considering the films containing γ-, η-, α-Al$_2$O$_3$, the addition of γ-Al$_2$O$_3$ showed better improvements in WVP (6.8 × 10^{-10} g/m s pa), while in case of addition of core@SiO$_2$ NP, α -Al$_2$O$_3$@SiO$_2$ resulted in better improvement in WVP (6.2 × 10^{-10} g/m s pa) compared with other types with SiO$_2$ as a shell. Regarding the films with core@TiO$_2$ NPs, η-Al$_2$O$_3$@TiO$_2$ revealed the best results (6.09 × 10^{-10} g/m s pa). These results were in good agreement with that of research done by Tajeddin (Tajeddin et al. 2019). CSNs depicted a better impact on WVP compared to all types of the allotropes of alumina (γ, η, and α). Coating SiO$_2$ and TiO$_2$ on the surface of the allotropes not only enhanced the surface area of the nanoparticles (Ghosh Chaudhuri and Paria 2012) but also they were capable of binding with hydrophilic groups within the CMC which prevent water vapor molecules from diffusion through the film (Gao et al. 2018).

WVP depends on two factors: the solubility and the diffusion of water molecules in the film matrix. By adding alumina nanocomposites, both of these parameters were affected. The presence of the nanoparticles among the CMC chains and bonding with them, which is causing the increase of the interconnection, alternatively reducing the mobility and the free spaces among the chains, that consequently the WVP of the films would be decreased. On the other hand, based on the previous statements, it was hypothesized that SiO$_2$ and TiO$_2$ nanoparticles reduced the solubility factor which consequently WVP decreased by reducing free OH groups in the film matrix (Lagaron et al. 2004; Ma et al. 2008).

Lagaron et al. (Lagaron et al. 2004) stated that a high-density network increases the inhibitory properties. Strong hydrogen bonds create zigzag pathways for the passage of water vapor molecules and cause low penetration of these molecules into the film, thereby reducing the permeability towards water vapor. Ma et al. (Ma et al. 2008) reported the

value of WVP through the pure starch film and the nanocomposite film containing 9% MCC about 5 × 10^{-10} g/m s pa and 2.5 × 10^{-10} g/m s pa, respectively. The researchers concluded that increasing CMC at concentrations greater than 9% increased the WVP of the films. The reduction of WVP in small amounts has been attributed to the creation of a complex pathway for water vapor molecules to pass due to better dispersion of nanoparticles. The researchers stated that the accumulation of particles in higher amounts of nanoparticles increases the WVP of the films. Based on the SEM results (Fig. 2), allotropes with no shell (TiO$_2$ and SiO$_2$) had the higher potential of agglomeration, thereby films with just allotropes showed a weak performance in WVP improvement. Chang et al. (Chang et al. 2010) reported about the WVP of the film with pure starch film (5.75 × 10^{-10} g/m s pa) and film with 5% nanocomposite cellulose (3.5 × 10^{-10} g/m s pa). The creation of a zigzag path for the passage of water vapor molecules by nanoparticles is explained in the film as the reason for this reduction. Saxena et al. (Saxena and Ragauskas 2009) investigated the WVP changes due to the integration of cellulosic whisker with xylan films. The results showed that films prepared with 10% sulfonated whiskers caused a reduction of 74% in WVP compared to pure xylan film. They also announced that the network of cellulosic whisker reduced WVP. Also, at the high whiskers values, agglomeration of whiskers creates channels in the film that allow water to penetrate faster.

Low permeability to gasses, especially oxygen gas, is very important in food packaging sensitive to aerobic microorganisms. Table 3 shows the GTR of the prepared films against oxygen. According to the results, addition of the allotropes of alumina decreased the GTR but this reduction was not significant (*P* > 0.05). Employing α-core@shell nanoparticles showed significant reduction in GTR (*P* < 0.05). Between η-Al$_2$O$_3$@TiO$_2$, showed a significant difference in GTR compared with η-Al$_2$O$_3$@SiO$_2$. Nanoparticles based on γ allotropes decreased the GTR but not significantly (*P* > 0.05). Comparing the nanoparticles in each column, simple form of the allotropes and alootropes with SiO$_2$ controlled GTR but not significantly. There was no significant difference between the final GTR (*P* > 0.05), while η-Al$_2$O$_3$@TiO$_2$ could show a significant difference compared with its γ and α form.

Table 3 GTR measurement for films incorporated with different types of Al_2O_3-based nanoparticles

Allotropes	GTR of films (cm^3/m^2d bar)			
	Without nanoparticle	-Al_2O_3	-Al_2O_3@SiO_2	-Al_2O_3@TiO_2
α	0.36 ± 0.02 [aA]	0.32 ± 0.02 [aA]	0.27 ± 0.01 [bA]	0.25 ± 0.01 [bA]
η	0.36 ± 0.02 [aA]	0.34 ± 0.02 [aA]	0.31 ± 0.01 [aA]	0.21 ± 0.01 [bB]
γ	0.36 ± 0.02 [aA]	0.30 ± 0.01 [bA]	0.29 ± 0.01 [bA]	0.28 ± 0.01 [bA]

Same letters means no significant difference (P value > 0.05); different letters means significant difference (P value < 0.05). Compare the small letter in each row and the capital letters in each column

As the results of GTR, the nanoparticle-based synthesized films have shown good barrier property against the permeation of oxygen. As is seen, with the addition of different nanocomposites to the film, the degree of GTR of nano-based films decreased significantly compared to the film without nanoparticle (0.36 cm^3/m^2d bar). Considering the addition of nanoparticles, γ-Al_2O_3 (0.30 cm^3/m^2d bar) revealed better improvement in GTR than α,η-Al_2O_3. Among the core@SiO_2 NP, α-Al_2O_3@SiO_2 depicted a significant reduction in GTR (0.27 cm^3/m^2d bar), and noticeably, η-Al_2O_3@TiO_2 showed the best performance in GTR reduction (0.21 cm^3/m^2d bar) compared with α,γ-Al_2O_3@TiO_2. Considering all types of nanoparticles, the best results in GTR regulation attributed to the film containing η-Al_2O_3@TiO_2.

Comparing the films containing just allotropes (no shell) and CSNs was inferred that CSNsnanoparticles resulted in better improvement in GTR. The reason might be their smaller size than the allotropes. Core@TiO_2 revealed higher productivity in GTR adjustment in contrast with core@SiO_2. Similar to WVP, based on the SEM results, core@TiO_2 nanoparticles showed a smaller diameter and less agglomeration, hence more dispersion and density in the film structure occurred. This high scattering, blocks or decreases the pathways for oxygen molecules diffusion into the film structure. Based on the results of XRD, core@SiO_2 resulted in an amorphous structure which consequently amorphous regions created, and this has been considered as a reason for facilitating oxygen transfer, while core@TiO_2 due to their high crystallinity resulted in more non-amorphous regions (Sepulveda et al. 2020). Similar results were reported by Branka et al. (Pilić et al. 2016) considering poly(lactic acid) containing SiO_2 NP. They also reported a reduction in oxygen diffusion in nano-based film compared with the neat films. They also reported that this improvement in barrier properties belongs to the uniform dispersity of nanoparticles. Vladimirov et al. (Vladimirov et al. 2006) also reported the significant effect of embedding silica nanoparticles on GTR of the polypropylene film. In general, fillers can be considered as an impermeable barrier to the movement of oxygen molecules. Based on the results, it can be imagined that the size of nanoparticles, uniform distribution, and lack of agglomeration affect the formation of the maze path of oxygen molecules through the polymer matrix. It should be noted that the formation of CSNs compared to conventional nanoparticles has a key role in improving the

dispersion and obtaining better results in this property. The use of these nanocomposites in films acts as a barrier against oxygen and can increase the shelf life of food and maintain its quality.

Conclusion

Nanoscience as a new technology has provided notable ways to improve food quality and control. This technology has created significant changes in the food packaging industry due to the modification of the molecular structure of materials. In this study, CSNs were synthesized using three allotropes of alumina (γ, α, and η) as the core, additionally TiO_2 and SiO_2 were employed as a shell to enhance the performance of food packaging. The effect of integration and intercalation of these nanoparticles with the packaging film was investigated. Consequently, the results showed that the films containing nanocomposite had a significant effect on moisture absorption, water vapor permeability, and showed high resistance towards permeability to oxygen gas compared to polymer films without nanoparticles. Among the synthesized nanocomposite, those containing η-Al_2O_3@TiO_2 and α-Al_2O_3@SiO_2 showed closed and the best performance.

Declarations

Conflict of Interest The authors declare no competing interests.

References

Ahangaran, F., & Navarchian, A. H. (2020). Recent advances in chemical surface modification of metal oxide nanoparticles with silane coupling agents: A review. *Advances in Colloid and Interface Science, 286*, 102298.

Ali, A. P. A. S., Mohammed, A. J., & Saud, H. R. (2018). Hydrothermal synthesis of TiO2/Al2O3 nanocomposite and its application as improved sonocatalyst. *International Journal of Engineering & Technology, 7*(4.37), 22–25.

Almasi, H., Ghanbarzadeh, B., & Entezami, A. (2009). Physicochemical properties of starch-CMC-nanoclay biodegradable films. *International journal of biological macromolecules, 46*, 1–5.

Almasi, H., Ghanbarzadeh, B., & Entezami, A. A. (2010). Physicochemical properties of starch-CMC-nanoclay biodegradable films. *Int J Biol Macromol, 46*(1), 1–5.

Amjadi, S., Emaminia, S., Nazari, M., Davudian, S. H., Roufegarinejad, L., & Hamishehkar, H. (2019). Application of reinforced ZnO nanoparticle-incorporated gelatin bionanocomposite film with chitosan nanofiber for packaging of chicken fillet and cheese as food models. *Food and Bioprocess Technology, 12*(7), 1205–1219.

Aswathanarayan, J. B., & Vittal, R. R. (2019). Nanoemulsions and their potential applications in food industry. *Frontiers in Sustainable Food Systems, 3*(95).

Baghani, M., Aliofkhazraei, M., & Poursalehi, R. (2015). Microwave-assisted sintering of Fe-Al2O3 nanocomposites: Study of corrosion and wear properties. *Procedia Materials Science, 11*, 689–694.

Basavegowda, N., Mandal, T. K., & Baek, K.-H. (2020). Bimetallic and trimetallic nanoparticles for active food packaging applications: A review. *Food and Bioprocess Technology, 13*(1), 30–44.

Biswal, A. K., & Misra, P. K. (2020). Biosynthesis and characterization of silver nanoparticles for prospective application in food packaging and biomedical fields. *Materials Chemistry and Physics, 250*, 123014.

Blanco, I. (2016). Lifetime prediction of food and beverage packaging wastes. *Journal of Thermal Analysis and Calorimetry, 125*(2), 809–816.

Blanco-Pascual, N., Koldeweij, R., Stevens, R., Montero, M., Gómez-Guillén, M., & Ten Cate, A. (2014). Peptide microencapsulation by core–shell printing technology for edible film application. *Food and bioprocess technology, 7*(9), 2472–2483.

Challagulla, N. V., Rohatgi, V., Sharma, D., & Kumar, R. (2020). Recent developments of nanomaterial applications in additive manufacturing: a brief review. *Current Opinion in Chemical Engineering, 28*, 75–82.

Chang, P., Jian, R., Zheng, P., Yu, J., & Ma, X. (2010). Preparation and properties of glycerol plasticized-starch (GPS)/cellulose nanoparticle (CN) composites. *Carbohydrate Polymers, 79*(2), 301–305.

Chen, H., Zhang, L., Hu, Y., Zhou, C., Lan, W., Fu, H., & She, Y. (2020). Nanomaterials as optical sensors for application in rapid detection of food contaminants, quality and authenticity. *Sensors and Actuators B: Chemical*, 129135.

Choudhury, B., & Choudhury, A. (2012). Luminescence characteristics of cobalt doped TiO2 nanoparticles. *Journal of luminescence, 132*(1), 178–184.

Chougala, L., Yatnatti, M., Linganagoudar, R., Kamble, R., & Kadadevarmath, J. (2017). A simple approach on synthesis of TiO2 nanoparticles and its application in dye Ssensitized solar cells. *Journal of Nano- and Electronic Physics, 9*, 04005–04001.

Cyras, V. P., Manfredi, L. B., Ton-That, M. T., & Vázquez, A. (2008). Physical and mechanical properties of thermoplastic starch/montmorillonite nanocomposite films. *Carbohydrate polymers., 73*(1), 55–63.

Das, C. G. A., Kumar, V. G., Dhas, T. S., Karthick, V., Govindaraju, K., Joselin, J. M., & Baalamurugan, J. (2020). Antibacterial activity of silver nanoparticles (biosynthesis): A short review on recent advances. *Biocatalysis and Agricultural Biotechnology, 27*, 101593.

Ding, H. L., Zhang, Y. X., Wang, S., Xu, J. M., Xu, S. C., & Li, G. H. (2012). Fe3O4@SiO2 core/shell nanoparticles: The silica coating regulations with a single core for different core sizes and shell thicknesses. *Chemistry of Materials, 24*(23), 4572–4580.

Dittanet, P., Pearson, R. A., & Kongkachuichay, P. (2017). Thermo-mechanical behaviors and moisture absorption of silica nanoparticle reinforcement in epoxy resins. *International Journal of Adhesion and Adhesives, 78*, 74–82.

Ergun, R., Guo, J., & Huebner-Keese, B. (2016). Cellulose. In B. Caballero, P. M. Finglas, & F. Toldrá (Eds.), *Encyclopedia of food and health* (pp. 694–702). Oxford, Academic Press.

Ernest Ravindran, R. S., Subha, V., & Ilangovan, R. (2020). Silver nanoparticles blended PEG/PVA nanocomposites synthesis and characterization for food packaging. *Arabian Journal of Chemistry, 13*(7), 6056–6060.

Ewing, C. S., Bhavsar, S., Veser, G., McCarthy, J. J., & Johnson, J. K. (2014). Accurate amorphous silica surface models from first-principles thermodynamics of surface dehydroxylation. *Langmuir, 30*(18), 5133–5141.

Farahmandjou, M., & Golabiyan, N. (2015). Solution combustion preparation of nano-Al2O3: Synthesis and characterization. *Transp Phenom Nano Micro Scales, 3*(2), 100–105.

Gaikwad, K., Singh, S., & Ajji, A. (2018). Moisture absorbers for food packaging applications. *Environmental Chemistry Letters, 17*.

Gao, Y., Liang, L., Zhao, S., Qi, Y., Zhang, W., Sun, X., Wang, Z., Wang, J., & Song, B. (2018). Hydrophilic and antimicrobial core–shell nanoparticles containing guanidine groups for ultrafiltration membrane modification. *RSC advances, 8*(44), 24690–24700.

García-García, I., Taboada-Rodríguez, A., López-Gomez, A., & Marín-Iniesta, F. (2013). Active packaging of cardboard to extend the shelf life of tomatoes. *Food and bioprocess technology, 6*(3), 754–761.

Ghosh Chaudhuri, R., & Paria, S. (2012). Core/shell nanoparticles: Classes, properties, synthesis mechanisms, characterization, and applications. *Chemical Reviews, 112*(4), 2373–2433.

Ghosh, R. S., Le, T. T., Terlier, T., Rimer, J. D., Harold, M. P., & Wang, D. (2020). Enhanced selective oxidation of ammonia in a Pt/Al2O3@ Cu/ZSM-5 Core–Shell Catalyst. *ACS Catalysis, 10*(6), 3604–3617.

Goetz, L., Mathew, A., Oksman, K., Gatenholm, P., & Ragauskas, A. J. (2009). A novel nanocomposite film prepared from crosslinked cellulosic whiskers. *Carbohydrate Polymers, 75*(1), 85–89.

Habibi, Y., & Dufresne, A. (2008). Highly filled bionanocomposites from functionalized polysaccharide nanocrystals. *Biomacromolecules, 9*(7), 1974–1980.

Hosseini, H., & Jafari, S. M. (2020). Introducing nano/microencapsulated bioactive ingredients for extending the shelf-life of food products. *Advances in Colloid and Interface Science, 282*, 102210.

Jafari, S., Jabari, S., Dehnad, D., & Shahidi, S. (2017). Heat transfer enhancement in thermal processing of tomato juice by application of nanofluids. *Food and Bioprocess Technology, 10*(2), 307–316.

Kavuncuoglu, H., Yalcin, H., & Dogan, M. (2019). Production of polyhedral oligomeric silsesquioxane (POSS) containing low density polyethylene (LDPE) based nanocomposite films for minced beef packaging for extension of shelf life. *LWT, 108*, 385–391.

Khalilullah, I., Reza, T., Chen, L., Placette, M., Mazumder, A. K. M. M. H., Zhou, J., Fan, J., Qian, C., Zhang, G., & Fan, X. (2018). In-situ characterization of moisture absorption and hygroscopic swelling of silicone/phosphor composite film and epoxy mold compound in LED packaging. *Microelectronics Reliability, 84*, 208–214.

Kumar, S., Mukherjee, A., & Dutta, J. (2020). Chitosan based nanocomposite films and coatings: Emerging antimicrobial food packaging alternatives. *Trends in Food Science & Technology, 97*, 196–209.

Kusumawati, D. H., Primary Putri, N., Hidayat, N., Taufiq, A., & Supardi, Z. A. I. (2018). Synthesis and characterization of γ-Al 2 O 3/SiO 2 composite materials. *JPhCS, 1093*(1), 012015.

Lagaron, J. M., Catalá, R., & Gavara, R. (2004). Structural characteristics defining high barrier properties in polymeric materials. *Materials Science and Technology, 20*(1), 1–7.

Lee, R., Kumaresan, Y., Yoon, S. Y., Um, S. H., Kwon, I. K., & Jung, G. Y. (2017). Design of gold nanoparticles-decorated SiO2@TiO2 core/shell nanostructures for visible light-activated photocatalysis. *RSC Advances, 7*(13), 7469–7475.

Lin, N., Yu, J., Chang, P. R., Li, J., & Huang, J. (2011). Poly(butylene succinate)-based biocomposites filled with polysaccharide

nanocrystals: Structure and properties. *Polymer Composites, 32*(3), 472–482.

Lipińska, M., Tomaszewska, M., & Kołożyn-Krajewska, D. (2019). Identifying factors associated with food losses during transportation: Potentials for social purposes. *Sustainability, 11*(7), 2046.

Liu, Z., Feng, Y., & Yi, X.-S. (1999). Thermoplastic starch/PVAl compounds: Preparation, processing, and properties. *Journal of Applied Polymer Science, 74*(11), 2667–2673.

López-Juárez, R., Razo-Perez, N., Pérez-Juache, T., Hernandez-Cristobal, O., & Reyes-López, S. Y. (2018). Synthesis of α-Al2O3 from aluminum cans by wet-chemical methods. *Results in Physics, 11*, 1075–1079.

Ma, X., Chang, P., & Yu, J. (2008). Properties of biodegradable thermoplastic pea starch/carboxymethyl cellulose and pea starch/microcrystalline cellulose composites. *Carbohydrate Polymers, 72*(3), 369–375.

Mishra, C., C. Ranjan Deo and S. Baskey (2020). "Influence of moisture absorption on mechanical properties of kenaf/glass reinforced polyester hybrid composite." Materials Today: Proceedings, 38, 2596, 2600

Moeller, M. and K. Matyjaszewski (2012). Polymer science: A comprehensive reference, Elsevier Science

Mohsin, M., Jawad, M., Yameen, M. A., Waseem, A., Shah, S. H., & Shaikh, A. J. (2020). An insight into the coating behavior of bimetallic silver and gold core-shell nanoparticles. *Plasmonics, 15*(6), 1599–1612.

Mrkić, S., Galić, K., Ivanković, M., Hamin, S., & Ciković, N. (2006). Gas transport and thermal characterization of mono-and di-polyethylene films used for food packaging. *Journal of applied polymer science, 99*(4), 1590–1599.

Mugundan, S., Rajamannan, B., Viruthagiri, G., Shanmugam, N., Gobi, R., & Praveen, P. (2015). Synthesis and characterization of undoped and cobalt-doped TiO2 nanoparticles via sol–gel technique. *Applied Nanoscience, 5*(4), 449–456.

Nakajima, H., Dijkstra, P., & Loos, K. (2017). The recent developments in biobased polymers toward general and engineering applications: Polymers that are upgraded from biodegradable polymers, analogous to petroleum-derived polymers, and newly developed. *Polymers, 9*(10), 523.

Nallathambi, G., Ramachandran, T., Venkatachalam, R., & Palanivelu, R. (2011). Effect of silica nanoparticles and BTCA on physical properties of cotton fabrics. *Materials Research, 14*(4), 552–559.

Neethirajan, S., & Jayas, D. S. (2011). Nanotechnology for the food and bioprocessing industries. *Food and bioprocess technology, 4*(1), 39–47.

Nithiyanantham, U., Zaki, A., Grosu, Y., González-Fernández, L., Igartua, J. M., & Faik, A. (2019). SiO2@Al2O3 core-shell nanoparticles based molten salts nanofluids for thermal energy storage applications. *Journal of Energy Storage, 26*, 101033.

Okuno, M., Zotov, N., Schmücker, M., & Schneider, H. (2005). Structure of SiO2–Al2O3 glasses: Combined X-ray diffraction, IR and Raman studies. *Journal of Non-Crystalline Solids, 351*(12), 1032–1038.

Pilić, B. M., Radusin, T. I., Ristić, I. S., Silvestre, C., Lazić, V. L., Baloš, S. S., & Duraccio, D. (2016). Hydrophobic silica nanoparticles as reinforcing filler for poly (lactic acid) polymer matrix. *Hemijska industrija, 70*(1), 73–80.

Prashanth, P. A., Raveendra, R. S., Hari Krishna, R., Ananda, S., Bhagya, N. P., Nagabhushana, B. M., Lingaraju, K., & Raja Naika, H. (2015). Synthesis, characterizations, antibacterial and photoluminescence studies of solution combustion-derived α-Al2O3 nanoparticles. *Journal of Asian Ceramic Societies, 3*(3), 345–351.

Rawtani, D., Rao, P. K., & Hussain, C. M. (2020). Recent advances in analytical, bioanalytical and miscellaneous applications of green nanomaterial. *TrAC Trends in Analytical Chemistry, 116109*.

Robertson, G. L. (2014). Food packaging. In N. K. Van Alfen (Ed.), *Encyclopedia of agriculture and food systems* (pp. 232–249). Oxford, Academic Press.

Sanchez-García, M. D. (2011). 21 - Carrageenan polysaccharides for food packaging. In J.-M. Lagarón (Ed.), *Multifunctional and nanoreinforced polymers for food packaging* (pp. 594–609). Woodhead Publishing.

Sangroniz, A., Zhu, J.-B., Tang, X., Etxeberria, A., Chen, E. Y. X., & Sardon, H. (2019). Packaging materials with desired mechanical and barrier properties and full chemical recyclability. *Nature Communications, 10*(1), 3559.

Saravanakumar, K., Sathiyaseelan, A., Mariadoss, A. V. A., Xiaowen, H., & Wang, M.-H. (2020). Physical and bioactivities of biopolymeric films incorporated with cellulose, sodium alginate and copper oxide nanoparticles for food packaging application. *International Journal of Biological Macromolecules, 153*, 207–214.

Saxena, A., & Ragauskas, A. (2009). Water transmission barrier properties of biodegradable films based on cellulosic whiskers and xylan. *Carbohydrate Polymers, 78*(2), 357–360.

Sepulveda, J., Villegas, C., Torres, A., Vargas, E., Rodriguez, F., Baltazar, S., Prada, A., Rojas, A., Romero, J., Faba, S., & Galotto, M. J. (2020). Effect of functionalized silica nanoparticles on the mass transfer process in active PLA nanocomposite films obtained by supercritical impregnation for sustainable food packaging. *The Journal of Supercritical Fluids, 161*, 104844.

Sharma, R., Jafari, S. M., & Sharma, S. (2020). Antimicrobial bio-nanocomposites and their potential applications in food packaging. *Food Control, 112*, 107086.

Shen, C.-H., & Springer, G. S. (1976). Moisture absorption and desorption of composite materials. *Journal of Composite Materials, 10*(1), 2–20.

Singh, T., Shukla, S., Kumar, P., Wahla, V., Bajpai, V. K., & Rather, I. A. (2017). Application of nanotechnology in food science: Perception and overview. *Frontiers in Microbiology, 8*(1501).

Siracusa, V., Blanco, I., Romani, S., Tylewicz, U., & Dalla Rosa, M. (2012). Gas permeability and thermal behavior of polypropylene films used for packaging minimally processed fresh-cut potatoes: A case study. *Journal of Food Science, 77*(10), E264–E272.

Souza, V. G. L., & Fernando, A. L. (2016). Nanoparticles in food packaging: Biodegradability and potential migration to food—A review. *Food Packaging and Shelf Life, 8*, 63–70.

Sun, X., Li, J., Zhang, F., Qin, X., Xiu, Z., Ru, H., & You, J. (2003). Synthesis of nanocrystalline α-Al2O3 powders from nanometric ammonium aluminum carbonate hydroxide. *Journal of the American Ceramic Society, 86*(8), 1321–1325.

Szkodo, M., Bien, A., & Antoszkiewicz, M. (2016). Effect of plasma sprayed and laser re-melted Al2O3 coatings on hardness and wear properties of stainless steel. *Ceramics International*, 42.

Tajeddin, B., Ramedani, N., & Mirzaei, H. (2019). Preparation and characterization of a bionanopolymer film for walnut packaging. *Polyolefins Journal, 6*(2), 159–167.

Thümmler, M., Motylenko, M., & Rafaja, D. (2019). Structure model of γ-Al 2 O 3 based on planar defects. *IUCrJ*, 6.

Turan, D. (2019). Water vapor transport properties of polyurethane films for packaging of respiring foods. *Food Engineering Reviews*.

Vladimirov, V., Betchev, C., Vassiliou, A., Papageorgiou, G., & Bikiaris, D. (2006). Dynamic mechanical and morphological studies of isotactic polypropylene/fumed silica nanocomposites with enhanced gas barrier properties. *Composites Science and Technology, 66*(15), 2935–2944.

Wang, L., Shao, S., Madebo, M. P., Hou, Y., Zheng, Y., & Jin, P. (2020). Effect of nano-SiO2 packing on postharvest quality and antioxidant capacity of loquat fruit under ambient temperature storage. *Food Chemistry, 315*, 126295.

Wong, E. H., & Rajoo, R. (2003). Moisture absorption and diffusion characterisation of packaging materials - Advanced treatment. *Microelectronics Reliability, 43*(12), 2087–2096.

Wu, X., Shao, G., Cui, S., Wang, L., & Shen, X. (2016). Synthesis of a novel Al2O3–SiO2 composite aerogel with high specific surface area at elevated temperatures using inexpensive inorganic salt of aluminum. *Ceramics International, 42*(1), 874–882.

Wynnyckyj, J., & Morris, C. (1985). A shear-type allotropie transformation in alumina. *Metallurgical Transactions B, 16*(2), 345–353.

Zhao, Y., Wu, R., Yu, H., Li, J., Liu, L., Wang, S., Chen, X., & Chan, T.-W. D. (2020). Magnetic solid-phase extraction of sulfonamide antibiotics in water and animal-derived food samples using core-shell magnetite and molybdenum disulfide nanocomposite adsorbent. *Journal of Chromatography A, 1610*, 460543.

Zhong, T., Oporto, G. S., & Jaczynski, J. (2017). 19 - Antimicrobial food packaging with cellulose-copper nanoparticles embedded in thermoplastic resins. In A. M. Grumezescu (Ed.), *Food Preservation* (pp. 671–702). Academic Press.

Zhu, Z., Cai, H., & Sun, D.-W. (2018). Titanium dioxide (TiO2) photocatalysis technology for nonthermal inactivation of microorganisms in foods. *Trends in Food Science & Technology, 75*, 23–35.

Zhu, Z., Zhang, Y., Shang, Y., & Wen, Y. (2019). Electrospun nanofibers containing TiO 2 for the photocatalytic degradation of ethylene and delaying postharvest ripening of bananas. *Food and Bioprocess Technology, 12*(2), 281–287.